LIGO AND VIRGO GRAVITATIONAL-WAVE DETECTORS AND THEIR SCIENCE REACH*

Damir Buskulic

LAPP, Université de Savoie, CNRS
BP 110, 74941 Annecy-Le-Vieux Cedex, France
buskulic@lapp.in2p3.fr

Ilya Mandel

School of Physics and Astronomy, University of Birmingham
Edgbaston, Birmingham B15 2TT, UK
imandel@star.sr.bham.ac.uk

(Received November 25, 2013)

Gravitational waves were predicted by Einstein in 1916 as wave solutions of the Einstein–Hilbert equations of General Relativity. Indirect experimental evidence of their existence was only obtained in the past 40 years, most famously through observations of the binary pulsar PSR 1913+16. Direct detection of gravitational waves is anticipated later this decade. It will be enabled by interferometric detectors Virgo and LIGO. We begin with a brief theoretical description and the historical background of the search for gravitational waves. We describe techniques used in interferometric detectors. We introduce the likely sources of gravitational waves and the foundations of data analysis. We briefly summarize key results to date and conclude with perspectives on future scientific payoffs.

DOI:10.5506/APhysPolB.44.2413
PACS numbers: 04.30.–w, 95.55.Ym, 95.85.Sz

1. Theoretical aspects

Looking at the consequences of General Relativity, Einstein identified already in 1916 the possibility of a wave solution to his equations in the weak field approximation. Physically, these solutions represent a perturbation of the metric propagating in a flat vacuum, empty of gravitational field sources.

* Presented at the LIII Cracow School of Theoretical Physics "Conformal Symmetry and Perspectives in Quantum and Mathematical Gravity", Zakopane, Poland, June 28–July 7, 2013.

In this chapter, we summarize the key theoretical aspects of gravitational waves; see, *e.g.*, [1–4] for more details.

1.1. Linearized General Relativity

1.1.1. Linearization of the equations

General Relativity equations (or the Einstein Field Equations) are non-linear equations. They can be expressed as

$$R_{\mu\nu} - \frac{1}{2} g_{\mu\nu} R = -\frac{8\pi G}{c^4} T_{\mu\nu} \,, \tag{1}$$

where $R_{\mu\nu}$ is the Ricci tensor, which is the contraction of the Riemann tensor and describes the space-time curvature, R the scalar curvature, contraction of the Ricci tensor, $g_{\mu\nu}$ the metric tensor and $T_{\mu\nu}$ the energy-momentum tensor which describes the energy-momentum content of space-time and is the source term of the equations.

It is natural to consider the conditions and approximations for which these equations would appear linear. These are the so-called weak field conditions, where the curvature is very close to the one of a flat Minkowski space-time. In these conditions, the metric can be written as

$$g_{\mu\nu} = \eta_{\mu\nu} + h_{\mu\nu} \,, \tag{2}$$

where $\eta_{\mu\nu}$ is a flat Minkowski space metric

$$\eta_{\mu\nu} = \begin{pmatrix} 1 & 0 & 0 & 0 \\ 0 & -1 & 0 & 0 \\ 0 & 0 & -1 & 0 \\ 0 & 0 & 0 & -1 \end{pmatrix} \tag{3}$$

and $h_{\mu\nu} \ll 1$ is a perturbation to this metric.

It is possible, in these conditions, to linearize Einstein's equations, or rewrite them considering only the first order, linear terms. In order to do that

- one linearizes the affine connexions by
  - — replacing $g_{\mu\nu}$ by $\eta_{\mu\nu} + h_{\mu\nu}$,
  - — not taking into account the higher order terms in $h_{\mu\nu}$,
- then, one linearizes the Riemann tensor.

The following equivalent equation is then obtained

$$\Box\bar{h}_{\mu\nu} + \eta_{\mu\nu}\partial_\rho\partial_\sigma\bar{h}^{\rho\sigma} - \partial_\nu\partial_\rho\bar{h}^\rho_\mu - \partial_\mu\partial_\rho\bar{h}^\rho_\nu = -2\frac{8\pi G}{c^4}T_{\mu\nu}\,, \tag{4}$$

where the "trace reverse" was defined as $\bar{h}_{\mu\nu} \equiv h_{\mu\nu} - \frac{1}{2}\eta_{\mu\nu}h$.

This equation may be simplified by using a particular gauge (a particular coordinate system), a harmonic gauge. Imposing gauge conditions is equivalent to using the invariance of the linearized Riemann tensor, hence the invariance of the intrinsic curvature, under infinitesimal coordinate transformations.

Under such a transformation

$$x'^\mu = x^\mu + \xi^\mu(x) \tag{5}$$

$h_{\mu\nu}$ becomes

$$h'_{\mu\nu} = h_{\mu\nu} - \partial_\mu\xi_\nu - \partial_\nu\xi_\mu \tag{6}$$

and by imposing gauge conditions, choosing $\xi^\mu(x)$ such that

$$\partial_\mu\bar{h}^{\mu\nu} = 0 \tag{7}$$

the field equations become much simpler

$$\Box\bar{h}^{\mu\nu} = -2\frac{8\pi G}{c^4}T^{\mu\nu}\,. \tag{8}$$

1.1.2. Gravitational waves in vacuum

Far away from any matter–energy content, in vacuum ($T_{\mu\nu} = 0$), the Einstein Field Equations become

$$\Box\bar{h}_{\mu\nu} = 0 \quad \Leftrightarrow \quad \left\{\frac{\partial^2}{\partial t^2} - \nabla^2\right\} h_{\mu\nu} = 0\,, \tag{9}$$

where the speed of light is $c = 1$. One recognizes a wave equation, which has solutions of the form

$$\bar{h}_{\mu\nu} = \mathrm{Re}\{A_{\mu\nu}\exp(ik_\rho x^\rho)\}\,. \tag{10}$$

The amplitude $A_{\mu\nu}$ and the wave vector k_ρ must satisfy the wave equation (9), giving the condition [2]

$$k_\rho k^\rho = 0 \tag{11}$$

which, developing the expression of k_ρ, gives

$$\omega^2 = c^2\,|k|^2$$

a dispersion relation indicating that the wave propagates at the speed of light c.

The amplitude and the wave vector should also satisfy the gauge condition $\partial_\mu \bar{h}_{\mu\nu} = 0$. Hence

$$k_\rho A^{\rho\sigma} = 0\,. \tag{12}$$

This condition reduces the number of independent elements of the amplitude $A_{\mu\nu}$ from 10 (4×4 symmetric matrix) to 6. We can further simplify the form of the amplitude by choosing a particular harmonic gauge such that

$$A_{0\sigma} = 0 \tag{13}$$

which gives 4 constraints and reduces the number of independent elements to 2. This particular gauge is called Transverse Traceless (TT). For a wave propagating in the z direction, the amplitude now reads

$$A_{\mu\nu} = \begin{pmatrix} 0 & 0 & 0 & 0 \\ 0 & A_{11} & A_{12} & 0 \\ 0 & A_{12} & -A_{11} & 0 \\ 0 & 0 & 0 & 0 \end{pmatrix}. \tag{14}$$

By choosing $A_{11} = 1$ and $A_{12} = 0$ (the so-called "+" polarization) or $A_{11} = 0$ and $A_{12} = 1$ ("×" polarization), one obtains two linear polarizations on which the general solution of the wave equation may be decomposed. If one chooses $A_{11} = 1$ and $A_{12} = \pm i$, one obtains two circular polarizations.

1.1.3. Proper distance between two test masses

In order to understand the effect of a gravitational wave on matter, since a single test mass cannot "feel" anything, we consider two such test masses, separated by a proper distance L (Fig. 1).

We can compute the proper distance while the wave is passing, supposing that the masses are separated by a coordinate distance Δx

$$L = \int_0^{\Delta x} dx \sqrt{-g_{xx}} = \int_0^{\Delta x} dx \sqrt{1 - h_{xx}^{\mathrm{TT}}(t, z=0)} \tag{15}$$

$$\approx \int_0^{\Delta x} dx \left[1 - \tfrac{1}{2} h_{xx}^{\mathrm{TT}}(t, z=0)\right] = \Delta x \left[1 - \tfrac{1}{2} h_{xx}^{\mathrm{TT}}(t, z=0)\right]. \tag{16}$$

The amplitude of the wave h is interpreted as the relative variation of the proper distance between two test masses.

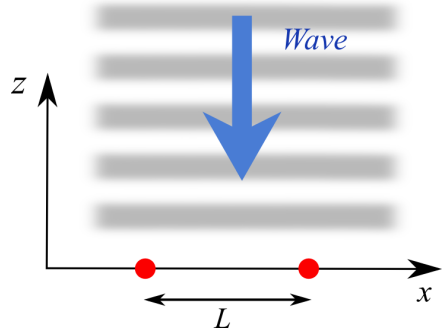

Fig. 1. Effect of a linearly polarized gravitational wave on two test masses initially separated by a distance L.

1.2. Effect of gravitational waves on matter

It is not possible to define the effect of gravitational waves on a single test particle: it would simply follow a geodesic and the values of the coordinates along its world line would not carry information. However, considering the relative motion of several neighboring test particles, we are able to see the effect of gravitational waves on matter. Let a set of such particles be distributed on a circle in the absence of the wave, in vacuum. Their motion is shown in figure 2 for a linear polarization of the wave and in figure 3 for a circular polarization. See [1, 3, 4] or [2] for the calculation of the effect.

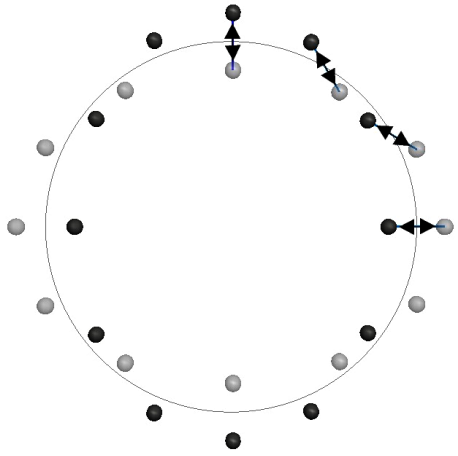

Fig. 2. Effect of a linearly polarized gravitational wave on a set of test masses arranged on a circle. Each mass has a simple harmonic motion with respect to its neighbors.

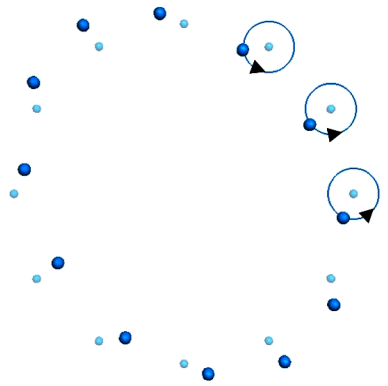

Fig. 3. Effect of a circularly polarized gravitational wave on a set of test masses arranged on a circle. Each mass has a circular motion centered on its initial position (in the absence of gravitational waves).

1.3. Generation of gravitational waves

In order to study the emission of gravitational waves by a moving mass distribution, we have to consider the complete Einstein equations, with the right-hand side containing the energy-momentum tensor

$$\Box \bar{h}_{\mu\nu} = -\frac{16\pi G}{c^4} T_{\mu\nu} \,. \tag{17}$$

We can, as in the case of electromagnetism, use the Green functions to obtain a solution in the form of a retarded potential

$$\bar{h}_{\mu\nu}(\boldsymbol{x}, t) = -\frac{4G}{c^4} \int\limits_{\text{source}} d\boldsymbol{x}' \frac{T_{\mu\nu}\left(\boldsymbol{x}', t - \frac{|\boldsymbol{x}-\boldsymbol{x}'|}{c}\right)}{|\boldsymbol{x} - \boldsymbol{x}'|} \,, \tag{18}$$

where $T_{\mu\nu}$ is the energy-momentum term of the Einstein field equations. We make the assumption that the source is isolated, compact (characteristic length R), far from the observer (*i.e.* $|\boldsymbol{x} - \boldsymbol{x}'| \gg R$) and moving slowly (speed v of its constituents with respect to each other $\ll c$). Then, it can be shown that the wave can be expressed in terms of the quadrupolar moment tensor of the source

$$\bar{h}_{ij}(t) = \frac{2G}{Rc^4} \frac{d^2 I_{ij}\left(t - \frac{R}{c}\right)}{dt^2} \,; \tag{19}$$

the quadrupolar moment tensor is

$$I_{ij}(t) = \int\limits_{\text{source}} d\boldsymbol{x}\; x_i x_j\; T_{00}(t, \boldsymbol{x}) \,, \tag{20}$$

where T_{00} is nothing else than the energy density of the source.

Contrary to the case of electromagnetism where a dipolar radiation can be produced when a charge density varies, this is not possible in the case of gravitation. Indeed, the equivalent of a dipolar radiation would be an oscillating motion of the center of density of an isolated energy distribution, which would violate the momentum conservation law. The gravitational radiation can be quadrupolar at best. The amplitude of quadrupolar radiation is, generally, much weaker than the dipolar one and this fact, together with the weak coupling of matter to gravity, explains why the amplitude of gravitational radiation is typically much weaker than that of electromagnetic radiation. The factor G/c^4 is of the order of $10^{-44}\,\mathrm{s^2 m^{-1} kg^{-1}}$; therefore, the only gravitational waves that we can hope to detect come from astrophysical sources with rapid motion of large, compact masses.

1.4. Generation example: binary system

Let us look at the simple case of a system of two compact objects orbiting around each other. As is shown in figure 4, we denote m_1 and m_2 the masses, a the distance between the two bodies, $M = m_1 + m_2$ the total mass and $\mu = m_1 m_2/M$ the reduced mass.

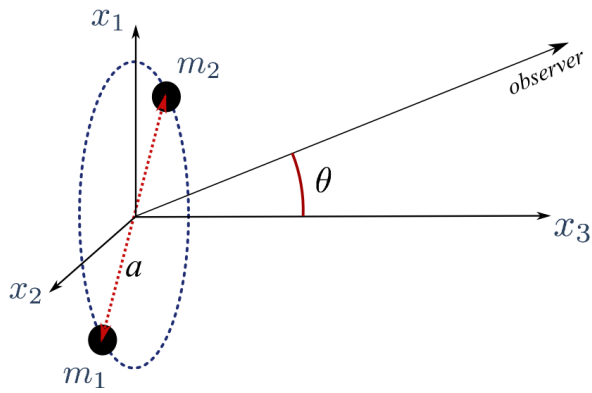

Fig. 4. Binary system of two compact objects in circular orbit around each other.

We consider circular orbits and a Newtonian approximation. We note the relative coordinates $x_1(t) = a\cos\omega t$, $x_2(t) = a\sin\omega t$, $x_3(t) = 0$. Kepler's third law gives the angular frequency corresponding to the frequency of rotation

$$\omega = \sqrt{\frac{GM}{a^3}}\,. \tag{21}$$

We can now compute h_+ and $h_\times$, the amplitudes of the two modes of the emitted wave, seen by an observer at a distance $R \gg a$ from the system, in the direction determined by the angle θ. One obtains

$$h_+(t) = \frac{4G\mu a^2\omega^2}{Rc^4}\frac{1+\cos^2\theta}{2}\cos 2\omega t\,, \tag{22}$$

$$h_\times(t) = \frac{4G\mu a^2\omega^2}{Rc^4}\cos\theta\sin 2\omega t\,. \tag{23}$$

Looking at two particular cases, illustrated in figure 5 (a), of an observer A (corresponding to $\cos\theta = 1$) and an observer B (corresponding to $\cos\theta = 0$), we notice the consistency of the observation with our intuition. Observer A "sees" the system perpendicularly to the plane of rotation ("face-on", figure 5 (b)) and measures a circular polarization, which is a combination of the two linear polarizations. Observer B sees a linear polarization as she observes the system in the plane of rotation ("edge-on", figure 5 (c)).

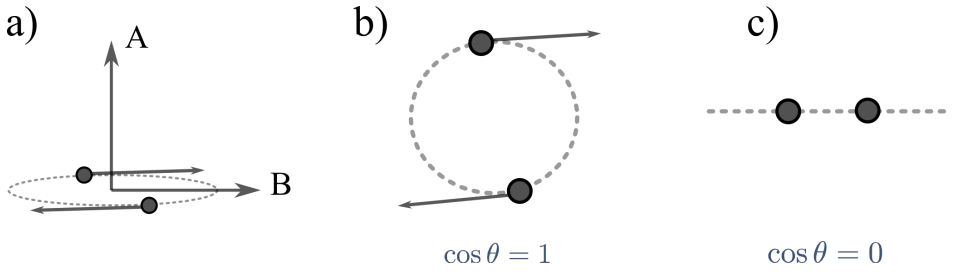

Fig. 5. Two observers in two particular directions A ($\cos\theta = 1$) and B ($\cos\theta = 0$) see either two linear polarizations (A), or only one (B).

The power radiated in gravitational waves per unit solid angle is given by

$$\frac{dP}{d\Omega} = \frac{2G\mu^2a^4\omega^6}{\pi c^5}\frac{1}{4}\left(1+6\cos^2\theta+\cos^4\theta\right)\,. \tag{24}$$

One notes $\mathcal{P}(\theta) = \frac{1}{4}(1+6\cos^2\theta+\cos^4\theta)$. We observe that there is an obvious axial symmetry in this expression and the power is non-vanishing whatever the direction of emission θ. It is maximal for the observer A, with $\mathcal{P}(0) = 2$ and minimal for the observer B, with $\mathcal{P}(\pi/2) = 0.25$.

The total radiated power is obtained by integrating over all angles

$$P = \frac{32G\mu^2a^4\omega^6}{5c^5}\,. \tag{25}$$

Here are a few examples and orders of magnitude:

- Sun–Jupiter system. The data are: Jupiter mass $m_{\mathrm{J}} = 1.9 \times 10^{27}$ kg, orbital radius $a = 7.8 \times 10^{11}$ m, angular frequency $\omega = 1.68 \times 10^{-7}\,\mathrm{s}^{-1}$. This gives the radiated power

$$P = 5 \times 10^{3}\ \mathrm{J/s}$$

  for comparison, the luminous power emitted by the sun is $L_{\odot} \sim 3.8 \times 10^{26}$ J/s.

- The binary pulsar PSR 1913+16 (Hulse and Taylor), emits a power

$$P = 7.24 \times 10^{24}\ \mathrm{J/s}\,.$$

The radiated energy is taken out of the orbital energy of the system, which, in turn, influences its evolution. Since the orbital energy decreases and is negative, the orbital radius decreases and the frequency of the gravitational waves increases. One can write an energy conservation equation, E being the total energy of the system

$$\frac{dE}{dt} = -P\,.$$

Since we are in the Newtonian case

$$E = -G\frac{m_1 m_2}{2a}\,, \qquad \omega^2 = \frac{GM}{a^3}\,, \tag{26}$$

hence the orbital diameter evolution equation

$$\dot{a} = -\frac{2}{3}(a\omega)\left(\frac{\dot{\omega}}{\omega^2}\right)\,.$$

In the above, $\dot{a}$ is the radial velocity, $a\omega$ the tangential velocity and the ratio $\frac{\dot{\omega}}{\omega^2}$ is called the adiabatic factor. In order to compute the waveform, we need to compute the gravitational wave frequency evolution. We start from expressions (26) and write the relation between the temporal derivative of E and the angular frequency ω

$$\dot{E} = G^{2/3}\frac{m_1 m_2}{2M^{1/3}}\frac{2}{3}\,\dot{\omega}\,\omega^{-1/3}\,.$$

Energy conservation yields

$$\dot{E} = -P \quad \Rightarrow \quad G^{2/3}\frac{m_1 m_2}{2M^{1/3}}\frac{2}{3}\,\dot{\omega}\,\omega^{-1/3} = \frac{32G\mu^2 a^4 \omega^6}{5c^5}$$

finally, we replace a by its expression as a function of ω to obtain the adiabatic factor

$$\frac{\dot{\omega}}{\omega^2} = \frac{96}{5}\frac{G^{5/3}}{c^5}\frac{\mu}{M}(M\omega)^{5/3}\,.$$

For what concerns the frequency of the gravitational wave emitted, the symmetry of the system implies that the wave frequency $f_{\rm GW}$ is twice the rotation frequency $\omega/(2\pi)$, which can be seen in the expressions of $h_+(t)$ (22) and $h_\times(t)$ (23). The frequency evolution equation of the emitted wave is

$$\dot{f}_{\rm GW} = \frac{96}{5}\frac{G^{5/3}}{c^5}\pi^{8/3}\mathcal{M}^{5/3}f_{\rm GW}^{11/3}\,, \tag{27}$$

where we define the "chirp mass"

$$\mathcal{M} = \mu^{3/5}M^{2/5}\,. \tag{28}$$

Figure 6 represents the computation of the wave amplitude as a function of the time of arrival at the detector. The amplitude of a frequency–domain representation of the waveform scales as $f^{-7/6}$, supposing a quasi-stationary (adiabatic) evolution of the system and keeping a Newtonian approximation.

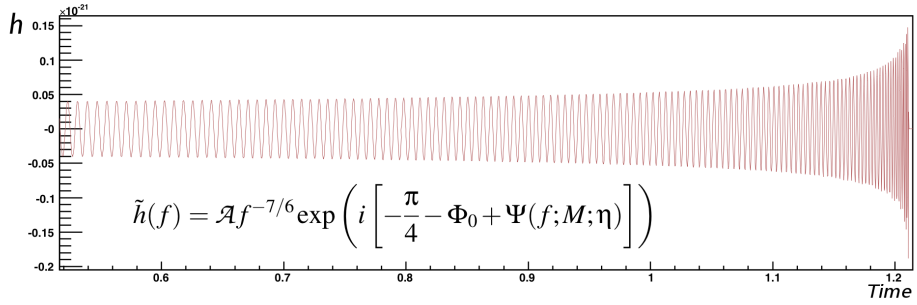

Fig. 6. Waveform produced by two interacting bodies in the inspiral phase, as it should be seen in an ideal detector.

A complete relativistic calculation cannot be made directly because of the non-linearity of the Einstein equations. But it is possible to compute a post-Newtonian perturbative expansion in the variable v^2/c^2 around the Newtonian limit, where v is the relative velocity of the two bodies ($v = (GM\omega)^{1/3}$).

Consider, for example, the expansion of the orbital phase in powers of the velocity

$$\phi(t) = \phi_{\rm ref} + \phi_N\sum_{k=0}^{n}\phi_{\frac{k}{2}{\rm PN}}(v/c)^k\,, \tag{29}$$

where $\phi_{\frac{k}{2}}$ are the successive coefficients, which incorporate higher-order effects such as the spin–spin interaction between the two objects or the spin–orbit interaction. We will not go into the details of the calculations [21].

In 1974, Russell Hulse and Joseph Taylor (University of Princeton) discovered a pulsar, PSR B1913+16, that they identified as being part of a binary system, the companion being a neutron star. This was a system of two compact objects orbiting around each other, that should emit gravitational waves, which would imply a decrease of the orbital period of the system. The calculations that we described allowed to verify experimentally the good agreement between the decrease of the period predicted by GR and the observations [5]. Hulse and Taylor received the 1993 Nobel prize for this discovery.

2. Detection by optical interferometry

In this chapter, we summarize the history and practical aspects of gravitational-wave detection. Further details and references can be found in the excellent reviews provided in [6, 7].

2.1. Historical aspects

In order to detect gravitational waves, the first idea was to use the mechanical resonance of a bar or a sphere. A wave that passes through the mechanical body should excite some proper modes of vibration. The first such detector was built by J. Weber at the University of Maryland in 1966. Weber declared that he has detected waves coming from the Galactic center (1968–1969) but other experiments did not observe anything and his assertion lost credibility.

Several resonant detectors were built since the 1970s, though only two of them (Auriga and Nautilus) run today in the so-called "astrowatch" mode. Because of the resonant character of the detection principle, the sensitive bandwidth of these detectors was $\Delta f \approx 50$–200 Hz. The central frequency was around 700 to 1000 Hz. Their maximal sensitivity is of the order of $h \sim 10^{-19}$ to 10^{-21}.

The second idea, that we are going to develop, is to measure the travel time of photons between two test masses. The principle of using a Michelson interferometer to do the measurement was first published by Gertsenshtein and Pustovoit in 1962 [8]. The first interferometer specifically built for the detection of gravitational waves was built by Forward *et al.* in 1971 [9]. The technical foundations of modern interferometers were developed by R. Weiss in 1972 [10].

2.2. Principle of detection for interferometric detectors

One of many excellent references for the basics of interferometric detection of gravitational waves is [6].

2.2.1. Basic ideas

We have shown the effect of a gravitational wave on a set of test masses arranged in a circle (figure 2). Let us suppose now that two of the test masses are replaced by the end mirrors of a Michelson interferometer (figure 7).

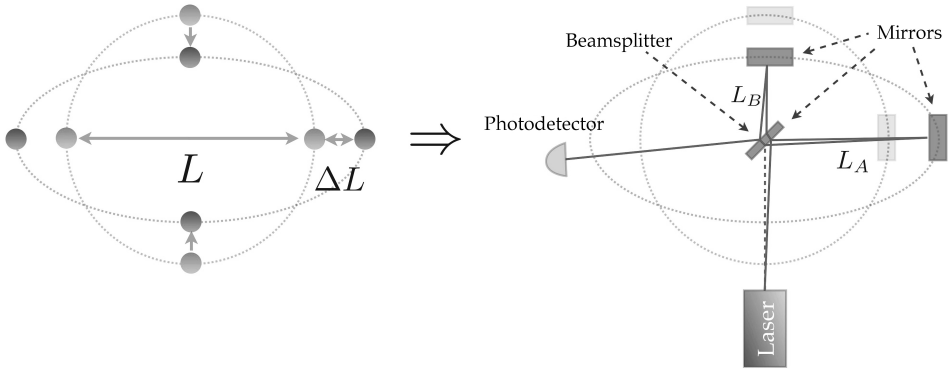

Fig. 7. Principle of the interferometric detection of gravitational waves. Two test masses of the thought experiment of figure 2 are replaced by mirrors, forming an interferometer with a beamsplitter at the center.

The passage of the gravitational wave is going to modify the distances between the beamsplitter and the mirrors and one will measure the optical path difference between the two arms. For this to work, the elements of the interferometer (mirrors, injection and detection systems) are suspended, we will later see how, and behave like freely falling masses in the interferometer plane, at least for frequencies $f \gg f_{\text{pend}}$, the resonance frequency of the pendulums.

In order to better understand the principle of detection, let us evaluate the round-trip time of the photons along one arm. In the general case, we can write the invariant line element for a photon in a gravitational field

$$ds^2 = 0 = g_{\alpha\beta}dx^\alpha dx^\beta = \eta_{\alpha\beta}dx^\alpha dx^\beta + h_{\alpha\beta}dx^\alpha dx^\beta \,. \tag{30}$$

In order to simplify the calculation, let us consider the particular case of a wave traveling along z, perpendicularly to the plane of the arms, and with a "+" polarization. We then get

$$ds^2 = 0 = -c^2dt^2 + (1 + h_+(t))dx^2 + (1 - h_+(t))dy^2 + dz^2 \,. \tag{31}$$

The time-of-flight of the photons is calculated by integrating on the path, for example along the "x" arm

$$\frac{1}{c}\int_0^L dx = \int_0^{\tau_{\text{one way}}} \frac{1}{\sqrt{1+h_+(t)}}\,dt \approx \int_0^{\tau_{\text{one way}}} \left(1-\frac{1}{2}h_+(t)\right)dt\,. \tag{32}$$

We then have to take into account

- the round trip along the arms,
- the wavelength of the gravitational wave, that we will suppose to be much bigger than the arms length. Hence, we will be able to consider that, on the path along the arm, the amplitude $h_+(t)$ is independent of the position,
- the period of the gravitational wave, that should be much greater than the light round trip time in one arm. Hence, we will consider that $h_+(t) = \text{constant} = h_+$.

We can now integrate along the "x" arm in two ways

$$\int_0^{\tau_{bfx}} \left(1-\frac{1}{2}h_+(t)\right)dt \approx \frac{1}{c}\left(\int_0^L dx - \int_L^0 dx\right) = \frac{2L_x}{c} \tag{33}$$

$$= \tau_{bfx} - \frac{1}{2}\int_0^{\tau_{bfx}} h_+(t)dt = \tau_{bfx} - \frac{1}{2}\int_0^{\frac{2L_x}{c}} h_+(t)dt \tag{34}$$

giving the round trip time

$$\Rightarrow \quad \tau_{bfx} = \frac{2L_x}{c} + \frac{1}{2}\int_0^{\frac{2L_x}{c}} h_+(t)dt\,. \tag{35}$$

The same calculation for the "y" arm gives

$$\Rightarrow \quad \tau_{bfy} = \frac{2L_y}{c} - \frac{1}{2}\int_0^{\frac{2L_y}{c}} h_+(t)dt\,. \tag{36}$$

What is really interesting is the time difference, where we consider h to be constant and $L_x = L_y = L$

$$\delta\tau_{bf} = \frac{1}{2}h_+ \left(\frac{2L_x}{c} + \frac{2L_y}{c}\right) = h_+ \frac{2L}{c}\,. \tag{37}$$

This time difference may be smaller than the laser light period. The interferometric device is actually sensitive to the phase shift between the light beams in the two arms. Thus, we rather consider the phase shift accumulated on the photons path

$$\delta\phi = \omega_{\text{laser}}\, \delta\tau_{bf} = \frac{4\pi}{\lambda_{\text{laser}}} L h_+\,. \tag{38}$$

It is interesting to note that this phase shift is proportional to h and L. We will try to design devices with the longest possible arms, leaving enough time for the light to "feel" the gravitational wave.

2.2.2. Angular response

For now, we have only considered waves coming along the "z" direction, perpendicular to the detector plane. If we consider a wave propagating along a direction (Θ, Φ) and with a polarization along the ψ angle, as shown in figure 8, the response of the interferometer reads

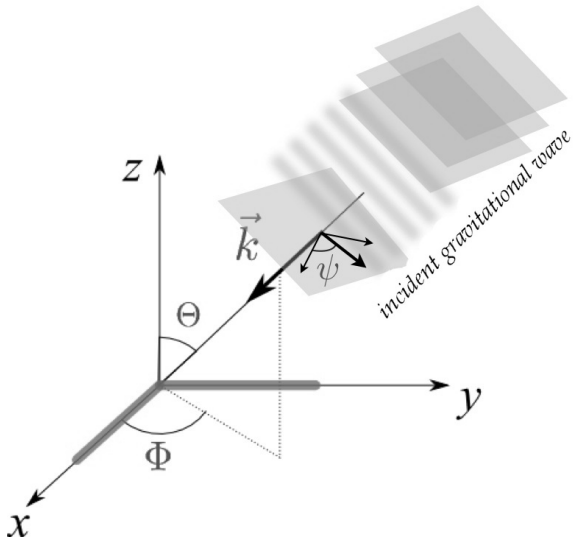

Fig. 8.

$$\frac{\Delta L}{L} = F_+(\Theta, \Phi, \psi)\; h_+ + F_\times(\Theta, \Phi, \psi)\; h_\times \tag{39}$$

where F_+ and $F_\times$ are the response functions for the two polarizations "+" and "×". These two functions are written

$$F_+ \;=\; -\tfrac{1}{2}\left(1+\cos^2\Theta\right)\cos 2\Phi\cos 2\psi - \cos\Theta\sin 2\Phi\sin 2\psi\,, \tag{40}$$

$$F_\times \;=\; \tfrac{1}{2}\left(1+\cos^2\Theta\right)\cos 2\Phi\sin 2\psi - \cos\Theta\sin 2\Phi\cos 2\psi\,. \tag{41}$$

Figure 9 illustrates the antenna pattern, which is the ratio of the interferometer response over the optimal response as a function of the direction of arrival of the wave, averaged over the possible polarizations of the wave. More precisely, this is $(F_+ + F_\times)/2$. We see that an interferometric detector is quasi omnidirectional (up to a factor 2), the response being null only in two directions, at 45° of the two arms in the detector plane.

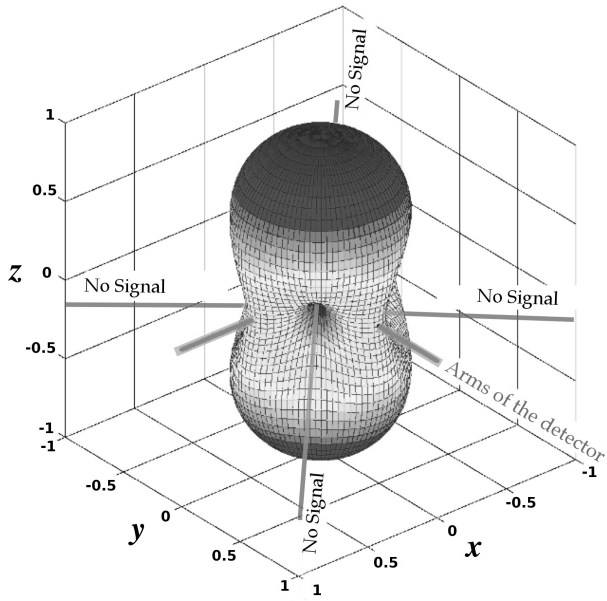

Fig. 9. Antenna pattern of an interferometer. The response is averaged over the polarization of the incoming wave, which travels along the direction (Θ, Φ).

2.2.3. The noise makes the detector

What are the limits in sensitivity of a detector? This is the point we are considering now. We will also greatly improve the simple optical scheme (Michelson) that we know.

The quantity that we measure on output of the interferometer is the phase difference $\delta\phi$ between the two optical paths followed by the light along the two arms. It is thus natural to ask what is the best tuning or working point of the interferometer. Let us look at the limits of our apparatus.

The ultimate limit is the shot noise. As one receives a given light power on the final photodetector, this corresponds to a given photon flux. If N photons hit the detector during a time T, the statistical variance will be $\sqrt{N}$ provided N is big, which is always the case. It is understandable in these conditions that the main limitations of the system will come from

- a limited laser power,
- an imperfect contrast,
- some noises coming from the laser itself, such as power fluctuations

and this is only the beginning ...

Without going too much into detail, we start from the noise power spectral density $S_b(f) = \sqrt{2h\nu P_{\mathrm{DC}}}$ $\mathrm{W}/\sqrt{\mathrm{Hz}}$ and define the "sensitivity" as the ratio of the photon-counting noise or shot noise (in $\mathrm{W}/\sqrt{\mathrm{Hz}}$) to the response of the interferometer (in W/m) normalized to the length L, giving

$$\sigma_h = \frac{1}{L}\sqrt{\frac{\hbar c\lambda}{4\pi P_{\max}}} \quad 1/\sqrt{\mathrm{Hz}}\,. \tag{42}$$

The longer the arms (L), the better the sensitivity (smaller σ_h). Since the physical length of the arms is limited by technology and cannot exceed several kilometers, a natural idea is to fold the arms so that the light makes a few round trips in each arm. It was found that the most effective and elegant way of achieving this goal is to introduce a Fabry–Perot cavity inside each arm (figure 10).

Fig. 10. Principle of a Fabry–Perot cavity used in Virgo and LIGO. The reflectivity of the input mirror is r_e, while the one of the end mirror is equal to 1.

For such a cavity, the average number of round trips for the photons is

$$\bar{N} = \frac{2\mathcal{F}}{\pi}\,, \tag{43}$$

where $\mathcal{F}$ is the finesse of the cavity. The sensitivity of the interferometer is improved by a factor $\bar{N}$

$$\sigma_h^{\mathrm{FP}} = \frac{\pi}{2\mathcal{F}L}\sqrt{\frac{\hbar c\lambda}{4\pi\, P_{\max}}}\, 1/\sqrt{\mathrm{Hz}}\,. \tag{44}$$

[This improvement applies only to shot noise, not other noise sources described below which accumulate with every bounce of light on the mirrors.]

Other improvements in the optical configuration (power recycling, mode cleaners, *etc.* ...) allow to reach the sensitivity needed for the detection of gravitational waves.

2.2.4. Improving the sensitivity, other sources of noise

The goal of most of the systems in LIGO and Virgo is, ultimately, to reduce the noises in the interferometer. In addition to the fundamental noise that we described above, there are several noise sources limiting the sensitivity in various frequency bands. We do not want to be comprehensive, but here are the main noise sources

- *Seismic noise*
  Dominant below a few Hz. It is due to the seismic activity which generates displacements of the mirrors affecting the length of the arms. In order to attenuate these displacements, the mirrors and some critical elements are suspended to attenuation systems. As an example, these systems allow for a typical attenuation of the movements of the mirrors of 10^{-9} at 4 Hz in Virgo.

- *Thermal noise*
  Between a few and a few hundred Hz, the dominant noises are the various thermal noises. The mechanical systems (suspension elements and mirrors) may be considered as oscillating systems of dissipative character. The thermal equilibrium with their environment introduces, according to the fluctuation–dissipation theorem, an uncertainty on their position. This uncertainty corresponds to the thermal noise. Depending on the mechanical system considered, the thermal noise covers a different frequency band. One finds most of the time a thermal noise spectral density covering a characteristic resonance of the system. This resonance depends on the quality factor Q of the system, that we will try to make as large as possible so as to reduce the noise spectral density outside of the peak.

- *Shot noise*
  Above a few hundred Hz, the shot noise becomes dominant. The presence of the Fabry–Perot cavities induces a rise of the noise at high frequency. This rise is due to the fact that the photons making several round trips in the arms, the optical length is not negligible anymore with respect to the wavelength of the gravitational wave, the cavities behave like lowpass filters with a cutoff frequency $f_c \approx 500$ Hz.

- *Instrumental noises*
  The presence of instrumental noises is mainly seen by an excess of noise between 3 and 100 Hz. Those are very diverse and they are very difficult to model. We can give some example: beam decentering introducing a coupling between angular and longitudinal movements of the mirrors, low intensity stray light, produced by diffusion of the beams on various elements, that is re-injected in the control loops, detection electronic noise, ... These technical noises are reduced during the commissioning phase after the detector is built.

2.2.5. Evolution of the sensitivity

As an illustration of the efforts made in the fight against the various noises, it is interesting to look at the evolution of the measured sensitivity

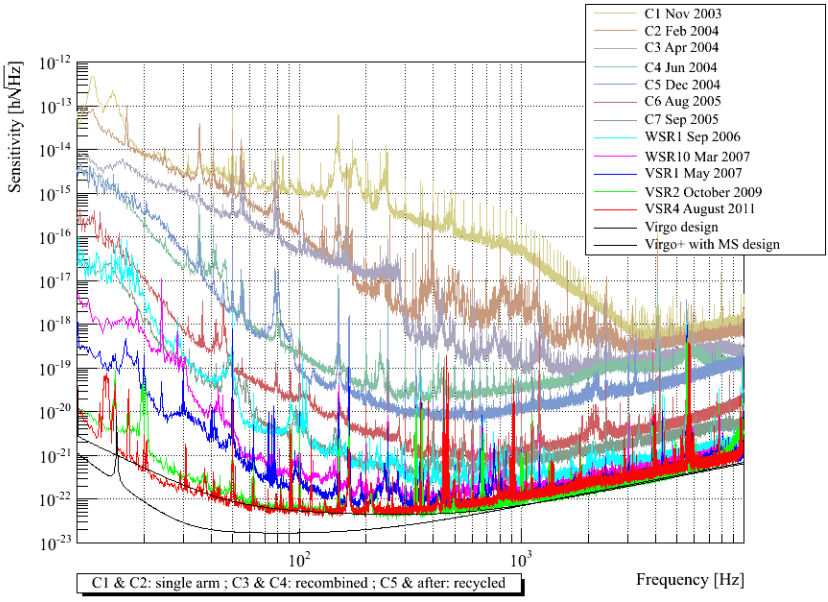

Fig. 11. Evolution of the sensitivity during the commissioning and scientific runs of Virgo [23].

of Virgo between November 2003 (date of the first technical run after the completion of the building of the instrument) and August 2011, date of the last scientific run (figure 11).

The improvements in sensitivity are due to the improvement of the optical configurations but also to the instrumental noise mitigation work.

3. Initial detectors and their planned upgrades

3.1. Virgo and LIGO: from initial to advanced detectors

The Virgo detector conducted four scientific runs with an improving sensitivity between May 2007 and September 2011. The LIGO detector had six science runs between August 2002 and October 2010. There was no detection in any of these runs. Virgo and LIGO are currently undergoing upgrade to future detectors called Advanced Virgo and Advanced LIGO. The goal of these upgrades is to improve the sensitivity by a factor of 10 with respect to the initial detectors. Since what is detected is the amplitude of the wave (and not the intensity), the accessible volume of space will scale as $1/(\text{sensitivity})^3$, which should improve the rate of potential events by a factor 10^3 [11]. Furthermore, improvements in low-frequency sensitivity (with the low-frequency wall decreasing from ~ 40 Hz for initial LIGO to ~ 10 Hz for Advanced LIGO) will enable searches for sources that are expected to emit in this previously inaccessible frequency band.

The improvements and changes foreseen and in preparation of Advanced Virgo include, among many others:

- an updated optical configuration with a signal recycling cavity;
- a 200 W laser with Gaussian beams and the waist in the middle of the Fabry–Perot cavities;
- a thermal compensation system because the mirrors undergo a deformation when the beam passes through it;
- heavier mirrors with a better surface quality (a flatness of 0.5 nm RMS) and an all fused silica assembly of the mirrors and the suspension fibers.

This should lead to a sensitivity curve like the one illustrated in figure 12 [24].

Advanced LIGO detectors will feature a variety of modifications and improvements, the most important of which are higher laser power (including power recycling) to reduce shot noise, and better passive and active suspensions for improved seismic isolation. To support these improvements, new technologies are needed, such as the thermal compensation system required to handle higher laser power. Other technological improvements include:

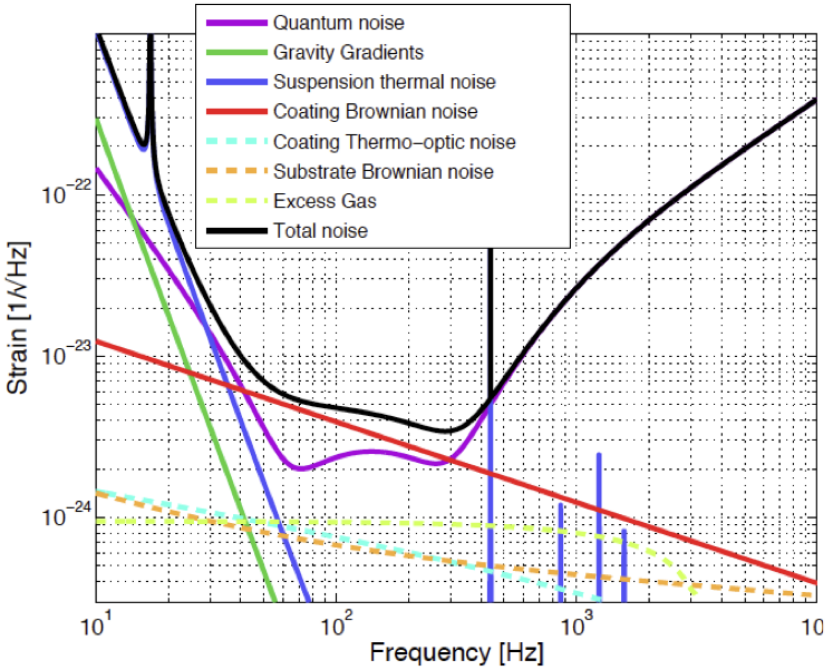

Fig. 12. Sensitivity curve foreseen for the Advanced Virgo upgrade.

- better optics to reduce scattering, including the use of shaped mirror and larger mirrors;
- a variety of techniques for mirror thermal noise mitigation, such as the employment of low-loss materials, in particular, all fused silica assembly of the mirrors, suspension fibers, and penultimate masses;
- improvements to the quality of the vacuum and baffles to reduce straight light scattering back into the detector;
- better mode cleaning; and
- power recycling to further reduce shot noise.

The addition of signal recycling will allow advanced LIGO detectors to be tuned to improve sensitivity in specific frequency bands.

One particularly interesting future upgrade (though not a feature included in the nominal advanced detectors) is the use of squeezed light to overcome the standard quantum limit. Despite their considerable mass, the end masses with attached mirrors are still governed by the Heisenberg uncertainty principle. As their positions are measured increasingly accurately,

their momenta are given a significant kick, which induces noise in future gravitational-wave measurements. The greater the laser power (and the lower the shot noise at high frequencies), the greater this radiation pressure noise at low frequencies. A way to get around this limitation is the injection of squeezed light, with correlations between the amplitude and phase fluctuations, through the dark part; frequency-dependent correlations could overcome the standard quantum limit.

Advanced detectors will have their first science runs in 2015–2016, but will require several stages of commissioning to achieve full design sensitivity. A possible scenario for observing and commissioning activities, indicating the typical evolution of sensitivity over the course of this decade, is presented in [25].

3.2. Worldwide network of detectors

Many of the scientific goals described in Section 6.2 require that the data analysis be made in common between several detectors. A coincident observation is necessary to provide confidence in a detection. Moreover, a single detector cannot determine the direction of the incoming wave, it can only provide a time of arrival. With three or more detectors distributed on the earth surface, it is possible to do a triangulation and reconstruct the incoming wave direction.

With this in mind, the signals coming from several detectors are analyzed jointly. The existing detectors that participated in the past scientific runs and the projects in construction that will participate in the future are the following:

- Virgo [12, 20], arm length 3 km, near Pisa, Italy.

- LIGO [13, 19], two 4 km long arms, one in Hanford (Washington state, U.S.) and the other in Livingston, near Baton Rouge (Louisiana, U.S.). On the same Hanford site and in the same vacuum tube, a second 2 km interferometer was operational until 2011. For Advanced LIGO, there will be only one interferometer in Hanford.

- GEO [14, 28], arm length 600 m, mainly used as a test bed for new technologies, but also currently in "astrowatch mode". It is located in Garching, Germany.

- Project KAGRA [16, 26], included in the worldwide network starting ∼2018, arm length 3 km, cryogenic underground detector (to reduce thermal and seismic noise), Japan. [Previously, a 300 m detector, TAMA [15], operated in Japan.]

- LIGO India is a developing project to bring one of the LIGO detectors to a 4 km site in India, starting in the $\sim$ 2019–2021 time frame.

The setup of a worldwide network of detectors will allow the confirmation of a detection, the determination of the position of a source, the decomposition of the polarization of the gravitational wave and also some studies that are impossible with a single detector like the study of a stochastic background of gravitational waves.

4. Types of sources

What are the likely sources of gravitational waves for ground-based detectors, whose peak sensitivity falls in the frequency band between a few tens and a few hundred Hz? In general, any configuration with a time-varying mass quadrupole moment can generate gravitational waves. However, in order to have a source that is detectable at significant distances, rapid motions of large, compact masses are necessary.

The frequency window sets a further constraint on observable sources. Very low-frequency signals (in the 10^{-9}–10^{-7} Hz band) can be observed with pulsar timing arrays; these include inspirals of supermassive ($> 10^7 M_\odot$) black-hole binaries. Space-born detectors such as the proposed (e)LISA mission are sensitive at frequencies of around a mHz, which makes them ideal for searching for mergers of massive ($\sim 10^6 M_\odot$) black-hole binaries, extreme mass ratio inspirals of stellar-mass objects into such massive black holes, and binaries of Galactic white dwarfs. Advanced LIGO and Virgo detectors, however, are sensitive only above 10 Hz. Main sequence stars and even white dwarfs are not sufficiently compact to sustain such high frequencies — they will be tidally disrupted or shredded if interactions in this frequency range are forced on them. In fact, only two types of astrophysical objects are known to be able to sustain such high frequencies: neutron stars and black holes. These are the most interesting astrophysical sources for advanced ground-based detectors.

LIGO and Virgo sources can be divided into continuous sources and transients; the latter can be further subdivided into sources involving a single object and those involving two objects.

Continuous or periodic sources include any long-lived signals from non-evolving or slowly evolving sources. These are likely to be nearly monochromatic (up to any modulations imposed by the relative motion of the detectors and the source), and are most likely to involve neutron stars with some form of deviation from axisymmetry that gives rise to a time-varying mass quadrupole moment. The simplest example is a neutron star with a "mountain" (perhaps some frozen-in crust deformation) or other fixed non-axisymmetric mass distribution that radiates away gravitational waves as it

rotates, very slowly losing energy and spinning down in the process. Other examples include a variety of oscillatory modes in the rotating neutron star, possibly driven by interactions with a companion, that give rise to continuous mass quadrupole variations.

The most violent single-object transient events are supernovae — the deaths of massive stars that have run out of nuclear fuel, are no longer able to sustain the internal pressure necessary to counterbalance self-gravity, and are collapsing into neutron stars or black holes while ejecting large amounts of mass and energy. Although spherically symmetric mass ejection will not give rise to gravitational waves (there is no variation of the mass quadrupole moment in this case), supernovae are known to be asymmetric because neutron star remnants are often seen to travel at speeds of a few hundred km/s, indicating a large kick to the remnant as a result of asymmetric mass-energy emission. In this case, some of the energy (perhaps only a part in 10^8 of the rest-mass energy, though there is significant uncertainty in this fraction) is emitted in gravitational waves. Other single-object transient events that could be accompanied by gravitational-wave emission include pulsar glitches and soft gamma repeater flares.

Perhaps the best-modeled LIGO and Virgo sources are binaries composed of two compact objects — binary neutron stars, binary black holes, or mixed neutron star — black hole systems. As discussed in Section 1.4, these binaries will spiral in as orbital energy is lost to gravitational-wave emission, increasing the amplitude and frequency of gravitational waves until the binary coalesces, producing a characteristic chirp signal in the process. Depending on their masses and the starting frequency assumed for the LIGO and Virgo sensitive bands, the sources can spend at most tens of minutes in the detector band. The duration of the inspiral in band starting from frequency f scales as $f^{-8/3}$; it also scales with the chirp mass as $M_c^{-5/3}$. That means that the most massive sources in the sensitive band of ground-based detectors — intermediate-mass black hole binaries weighing in at a few hundred solar masses — will be very fast transients indeed, lasting for only a few seconds in band.

Much work has gone into modeling the waveforms from compact binaries. As discussed in Section 1.4, the early portion of the inspiral can be modeled as a post-Newtonian expansion in the v/c parameter. After a black hole has formed as a result of the merger, it will need to get rid of excess "hair" before settling down to the stationary Kerr metric; the quasi-normal modes of gravitational-wave emission during the ringdown process have been studied perturbatively. Finally, the merger itself has long avoided analytical solutions — but breakthroughs in numerical relatively, *i.e.*, numerical solutions of non-linear Einstein equations that require significant computational resources, have enabled late inspiral and merger waveforms to be

computed. Now, analytical waveform families tuned to numerical–relativity results can reproduce the full gravitational wave train, though further work is required to make these waveforms more accurate and to include more complex effects, such as precession when the binary companions have spins that are misaligned from the orbital angular momentum, eccentricity, and intermediate mass ratios of $\sim$ 10–100:1.

Of course, the goal of advanced Virgo and LIGO instruments is to make a detection with the achieved sensitivity, so we want to know how likely this is for binary sources. This requires an estimate of the merger rate of these binaries in the Universe. We can give the most confident answer for neutron-star binaries, where two types of empirical observations provide evidence of merger rates. The first are binary pulsars in our Galaxy. The second are short gamma ray bursts.

Binary pulsars of interest to us, which include the famous Hulse–Taylor pulsar, are systems where a pulsing neutron star is in a close orbit around a companion which is another neutron star — sufficiently close that the system will merge in less than a few billion years though the emission of gravitational waves. Only $\sim$ 5 such systems are known in our Galaxy, so small-number statistics provide one source of uncertainty. Another source of uncertainty is our imperfect knowledge of the luminosity distribution of pulsars. Radio observations of binary pulsars are only possible in our own Galaxy, so rates must be extrapolated to the rest of the Universe.

Meanwhile, short gamma ray bursts are extremely energetic cosmic explosions that are believed (but are not yet proven) to be associated with mergers of binary neutron stars or neutron star — black hole binaries. In addition to the uncertain association itself, other sources of uncertainty include the poorly known beaming factor of short gamma ray bursts and difficulties in estimating the selection effects connected to their observability. Recent estimates of the beaming factor with jet breaks yield rates that are in broad agreement with Galactic binary pulsar observations.

Overall, rates of between 1 and 1000 binary neutron star mergers per million years in our Galaxy may be plausible. This range translates into an expected detection rate of between one binary neutron star every two years and one binary neutron star per day for the advanced detector network operating at design sensitivity.

No direct observations of black hole binaries exist, but the merger rates of such systems (as well as neutron star — black hole binaries) can be estimated through computer models of the evolution of large sets of isolated stellar binaries. Model uncertainties again give large ranges in possible merger rates, which are, generally, lower than those of binary neutron stars. However, more massive sources emit higher-amplitude gravitational waves, which can be detected at larger distances. Therefore, binary black-hole detection rates

fall into similar ranges as binary neutron star detection rates. Furthermore, merger rates from isolated binaries can be enhanced by accounting for dynamical binary formation in dense stellar environments such as globular clusters and galactic nuclear stellar clusters. More details on merger and detection rate estimates are available in [11, 29] and references therein.

Other gravitational-wave sources could include stochastic backgrounds from a large number of individually unresolvable astrophysical sources belonging to any of the categories described above, or stochastic backgrounds of cosmological origin, perhaps associated with early-Universe phase transitions or cosmic string cusps. And, of course, we always want to be on the lookout for exciting discoveries of the unexpected!

5. Searches

Gravitational waves couple very weakly with our detectors, and leave an imprint that may be much smaller than the magnitude of the noise. Is there any hope to pull out the weak signal that is buried in the noise — to extract the proverbial needle from the haystack? And, if so, how can this be done most effectively?

The full answer to this question is a topic of many Ph.D. dissertations and continuing research. Here, we will attempt to provide the general flavor of the kinds of techniques that are used. We will focus on searches for transients of astrophysical origin in gravitational-wave data; somewhat different but related techniques are required to search for periodic sources or for stochastic backgrounds.

We can consider the data set $d(f)$ (which we will write in the frequency-domain for simplicity — this simply assumes that the data and waveforms have been Fourier-transformed to the frequency domain) as a sum of a signal $h(f)$ and noise $n(f)$

$$d(f) = h(f) + n(f)\,. \tag{45}$$

The noise is assumed to be stationary and Gaussian, allowing us to represent it via a noise power spectral density $S(f)$. Formally,

$$E\left[n(f)n^*\left(f'\right)\right] = S(f)\delta\left(f - f'\right)\,. \tag{46}$$

There are two basic ways to look for the signal in the data: one which is based on accurate signal models (modeled searches), and one which does not rely on such models, but only assumes some general behavior such as the fact that multiple instruments in a network should (nearly) simultaneously observe the same gravitational wave signal (unmodeled searches). The difficulty in both cases is to distinguish the signal from the noise background.

Modeled searches can use the constraints provided by the model to separate the signals from the noise background. If a signal is expected to have a very particular set of features — say, the chirping behavior expected for an inspiraling binary — it may be possible to extract it even from overwhelming noise: although noise may be loud, it is very unlikely to perfectly reproduce the expected signal model. When a model is available, it can be shown that there is an optimal way to search for the signal by filtering the data against the signal — *i.e.*, sliding the signal model against the data until a good match is observed. The signal-to-noise-ratio (SNR) of this optimal matched filter is the ratio of the expected output of the filter when a signal is present to the standard deviation of the filter output when pure noise is being filtered. For data d and signal model h, the SNR ρ of the optimal Wiener filter is

$$\rho = \frac{\langle d|h\rangle}{\sqrt{\langle h|h\rangle}}\,, \tag{47}$$

where

$$\langle a|b\rangle = 4\Re \int_0^\infty \frac{a(f)b^*(f)}{S(f)} df\,. \tag{48}$$

Of course, we do not have just a single possible signal — we do not know *a priori* whether the data may contain a binary neutron star or a binary black hole, and precise choices of companion masses and spins influence the exact signal model. If we denote the signal parameters (masses, spins, *etc.*) as $\vec{\theta}$, then there is a whole family of signal models to consider, $h(\vec{\theta}; f)$. We operate with a discrete set of such signal models, each known as a template, chosen to be dense enough that we would be unlikely to miss a detection simply because of the finite density of this set, or bank, of templates. The maximum SNR is then computed by maximizing SNRs over all templates in the bank. SNRs of multiple instruments in a network that make a simultaneous (coincident) observation are added in quadrature to provide a ranking statistic for determining the level of confidence in a candidate event as a possible gravitational-wave detection.

Modeled searches tend to be computationally intensive because of the cost of template waveform computation. More worryingly, if template waveforms are imperfect, or if no waveforms exist for an unanticipated signal, the signal can be missed altogether. Running unmodeled searches in parallel with modeled searches provides confidence that such unexpected signals will not be missed. Unmodeled searches typically rely on overall excess power, relative to that expected in background noise alone, concentrated in the time-frequency plane. Although details of how this excess power is measured and reconstructed differ for different search models, all unmodeled searches are typically sensitive to a broad class of signals and relatively

computationally inexpensive. They also make good use of coherence between the data streams of different detectors in the network. Unmodeled searches may have lower resolving power than modeled searches because of the lack of additional information to discriminate signal from noise; however, when the signal model is relatively poor in features (*e.g.*, for short signals that are expected to last only a few cycles in band, such as signals from mergers of intermediate-mass black hole binaries), unmodeled searches can be very competitive with modeled searches.

In practice, detector noise is not perfectly stationary and Gaussian. It has a variety of artifacts: occasional spikes and other transient features, commonly known as glitches. Sometimes, the origins of these glitches are well-understood: for example, they may be caused by physical phenomena such as unusually high levels of seismic noise that couple into the detectors. Auxiliary environmental channels can be used to trace these artifacts, and data quality vetoes ensure that untrustworthy data are not analyzed. Not all glitches are caught by such vetoes, but although surviving glitches may yield loud, high-SNR triggers, glitch events do not necessarily look like true signals: for example, they may have the wrong distribution of power across different frequencies. Therefore, in addition to SNR (which would be the best discriminator if the noise were truly stationary and Gaussian), other measures are used to construct more robust statistics for distinguishing signals from background.

Yet the question remains: if the data are known to be glitchy, can we ever be truly confident that a putative detection with a loud ranking statistic is not due to an unusual noise event? Gaining this certainty requires a robust mechanism for estimating the distribution of our ranking statistics in the background. However, any stretch of our data *could* host a signal, and we do not know *a priori* whether to classify it as signal or noise — so how can the noise background be estimated? This is where multiple detectors in a network are crucial. While any signal is expected to appear in all detectors within the gravitational-wave travel time between them, *i.e.*, within 40 ms of detectors located on Earth, noise events should not be correlated between detectors. Therefore, sliding data from multiple detectors against each other — say, carrying out a search of data from one of the LIGO detectors today in fake coincidence with data taken at Virgo yesterday — allows us to look for noise-only events in the expectation that no simultaneous astrophysical signals would appear. Many different background realizations can be created by sliding detector data by different time shifts. Suppose that data are taken over the course of a year, and searched along with 1000 years of background data that are generated with 1000 independent time slides. If the physical, non-time-shifted data contain an event with a ranking statistic louder than anything appearing in the 1000 years of background, we know that the rate

at which such events could be generated by noise alone is less than 1 in 1000 years. That, along with careful scrutiny of the data, auxiliary channels, and a variety of follow-up analyses, may give us sufficient confidence to declare the first detection of gravitational waves.

One of the follow-up analyses that we would undertake with a plausible candidate signal is an attempt to extract the physical parameters of the source form the data. Crude parameter estimation is already provided by a modeled search: if the template $h(\vec{\theta})$ yields the highest SNR, then the signal parameters are probably somewhere in the vicinity of $\vec{\theta}$. However, this does not give us information about just how accurately these parameters can be measured; moreover, we could miss possible degeneracies in the parameter space, which is typically multidimensional (15 parameters are needed to describe a compact binary with spinning components) and sometimes multimodal.

A more careful exploration of the parameter space is therefore in order. We begin by considering the likelihood that a given data set could be generated if the parameters were known. This is given by the probability of generating a particular realization of the noise equal to the difference between the data and the model

$$p\left(d|\vec{\theta}\right) \propto e^{-(1/2)\left\langle d-h\left(\vec{\theta}\right)\middle|d-h\left(\vec{\theta}\right)\right\rangle}. \tag{49}$$

[Note that maximizing this likelihood is equivalent to minimizing the noise-weighted residuals.] Then, Bayes' rule can be used to convert this likelihood into a posterior on the source parameters of interest

$$p\left(\vec{\theta}\,|d\right) = \frac{p\left(d|\vec{\theta}\right)p\left(\vec{\theta}\right)}{p(d)}, \tag{50}$$

where $p(\vec{\theta})$ is the prior and $p(d)$ is the evidence, a normalization factor. In principle, this approach is sufficient for reconstructing the posterior probability distribution function on the signal parameters given the data. In practice, the large dimensionality of the parameter space and its complex structure mean that sophisticated stochastic techniques are necessary to efficiently explore the high-dimensional parameter space without getting stuck on local maxima. Techniques such as parallel tempered Markov-chain Monte Carlo and several variants of nested sampling have been successfully applied to the problem of parameter estimation on gravitational-wave signatures of coalescing compact binaries.

6. Main results and future perspectives

6.1. Results from initial Virgo and LIGO

Initial LIGO and Virgo have not made any detections of gravitational waves. For many source types, this was anticipated, as any detection would have required a great deal of serendipity. For example, even the most optimistic plausible predictions for binary neutron star merger rates correspond to only one detection in 5 years at the sensitivity of initial detectors, so the lack of a detection is not surprising. Conversely, the upper limits on merger rates provided by initial detectors are above the optimistic astrophysical predictions and, hence, do not aid in constraining astrophysical models of binary evolution.

However, other non-detections by initial detectors have been of astrophysical interest. We provide three examples here:

- Short gamma ray burst GRB070201 overlapped the Andromeda galaxy (M31), located at a distance of ~ 770 kpc. A search of the data at the time of the burst was able to rule out a binary coalescence in M31 at a confidence $> 99\%$ [22].

- The best upper limit to date has been placed on the density of the stochastic background energy density at a frequency of 100 Hz: $\Omega_0 < 6.9 \times 10^{-6}$ in units of the closure density of the Universe [27].

- The Crab and Vela pulsars are observed to spin down, so they must be losing energy; potentially, a significant fraction of this energy could be emitted as gravitational waves. However, upper limits have surpassed the spindown limit for both pulsars, and the limit for the Crab shows that no more than 2% of its energy emission could be in gravitational waves [30].

6.2. Future perspectives: scientific payoffs

Advanced LIGO and Virgo are expected to usher in the era of gravitational-wave astronomy. We anticipate not just the first direct detection of gravitational waves, but the opportunity to use them as new tools to probe cosmology, fundamental physics, and astrophysics.

Gravitational waves can provide an alternative tool for probing the distance ladder and exploring cosmology. Cosmology with electromagnetic sources relies on standard candles, such as Type 1A supernovae — objects whose absolute luminosity is constant or easily estimated from other properties, so that measurements of apparent luminosity can be used to infer

distances. Meanwhile, gravitational-wave sources are standard sirens: the distance information is directly encoded into the gravitational-wave signature. However, unlike with electromagnetic sources, redshifts cannot be extracted directly from gravitational-wave observations, as they are degenerate with mass parameters. To extract redshift, one must rely on either direct associations with electromagnetic counterparts, or statistical associations with host galaxies. Alternatively, it may be possible to break the mass-redshift degeneracy in systems with matter (neutron stars), or this degeneracy may prove to be surmountable if the intrinsic mass distribution of coalescing binary neutron stars is sufficiently narrow. We do not expect that advanced LIGO and Virgo will be competitive with other techniques for precision cosmology; nevertheless, because these observations will not suffer from the same systematics that may plague other measurements, they may turn out to be an extremely useful check on cosmography.

Gravitational waves provide direct probes of dynamically evolving spacetimes with strong gravitational fields. Binaries will reach significant fractions of the speed of light before coalescence. High-mass-ratio inspirals involve many orbits within a distance of a few Schwarzschild radii of the black-hole horizon, and the spacetime signature will be imprinted on the emitted gravitational waves. These regimes are simply not accessible through other means. Thus, gravitational-wave observations will enable precise and otherwise unachievable tests of strong-field gravity, including the no-hair theorem (or, more properly, the cosmic censorship conjecture and the supposition that all sufficiently massive ultra-compact objects are Kerr black holes) and the theory of general relativity itself.

Gravitational waves will also probe the properties of extremely dense matter in neutron stars. Sufficiently late in their inspiral, neutron stars cease to behave as point particles and exhibit signatures of tidal interaction and tidal energy dissipation, changing the rate of orbital evolution and gravitational-wave emission. Therefore, gravitational waves from binaries that include neutron stars carry information about the neutron star tidal deformability and equation of state. Because gravitational waves are sensitive to bulk properties of objects, rather than the surface properties that are directly accessible with traditional electromagnetic astronomy, this provides complementary information about the fundamental physics of ultra-dense matter.

Of course, LIGO and Virgo are astrophysical observatories, and there is great hope that they will enable significant advances in astronomy, either jointly or with other observations.

Multi-messenger observations are possible with electromagnetic or neutrino observatories. These can proceed in two directions: either *(i)* in-depth searches of archival gravitational-wave data can be motivated by electromagnetic transient discoveries, or *(ii)* gravitational-wave triggers can be followed up with other telescopes to search for electromagnetic counterparts. Both studies have been pursued in the past. For example, during the 2009–2010 science run, a search for gravitational-wave signals associated with 154 gamma ray bursts was conducted, of which 26 were short [17]. Meanwhile, during the last initial LIGO and Virgo science runs, a few plausible gravitational-wave candidates (none of which were eventually confirmed as detections) were sent out within ~ 30 minutes to a dozen partners [18]. Such multi-messenger observations could, for instance, confirm that short gamma ray burst are, in fact, associated with binary neutron star mergers.

Although a multi-messenger observation may not be very likely in the next few years, there is great potential for gravitational-wave astrophysics to make discoveries in the absence of any counterparts. Individual observations could prove extremely exciting. For instance, a detection of a binary component with a measured mass of 150 ± 20 solar masses would yield the first proof of the existence of intermediate mass black holes in this mass range. A high-eccentricity binary would almost surely indicate the importance of dynamical interactions in compact binary formation and evolution.

Meanwhile, advanced LIGO and Virgo may detect tens or even hundreds of binary neutrons stars and binary black holes. The rates and mass distributions of these observed systems will then be compared to population synthesis models in order to gain an insight into the astrophysics of stellar and binary evolution. With these observations, we hope to learn more about the life and death of massive stars, investigate the elusive physics of common envelopes, and understand the fallback mechanisms and natal kicks that accompany the birth of black holes. We will also look for signatures of multiple subpopulations in order to identify isolated binaries and dynamically formed systems, explore the time delays between binary formation and merger, and probe the mass gap between neutron stars and black holes.

Beyond these plans, we can consider a number what-if scenarios. Could a massive neutron star or a very low mass black hole be detected and force us to re-evaluate our models of stellar evolution? LIGO and Virgo could detect a pulsar with a significant ellipticity, or vibrational modes in an accreting neutron star in a binary. And might we be lucky enough to detect gravitational waves from a nearby supernova that would help us resolve persisting mysteries in the mechanisms of these explosions? Potential discoveries await!

We thank S. Fairhurst, J. Harms, D. Shoemaker, and other colleagues in the Virgo Collaboration and LIGO Scientific Collaboration for useful comments.

REFERENCES

[1] R.M. Wald, *General Relativity*, The University of Chicago Press, 1984.

[2] M.P. Hobson, G.P. Efstathiou, A.N. Lasenby, *General Relativity: An Introduction for Physicists*, Cambridge University Press, 2006.

[3] S. Carroll, *Spacetime and Geometry: An Introduction to General Relativity* Addison-Wesley, 2003.

[4] J.L. Martin, *General Relativity: a First Course for Physicists*, Prentice Hall, 1996.

[5] J.M. Weisberg, J.H. Taylor, *Astrophys. J.* **576**, 942 (2002).

[6] P.R. Saulson, *Fundamentals of Interferometric Gravitational Wave Detectors*, World Scientific, 1994.

[7] M. Pitkin, S. Reid, S. Rowan, J. Hough, *Living Rev. Relativity* **14**, 5 (2011).

[8] M.E. Gertsenshtein, V.I. Pustovoit, *Sov. Phys.* **253**, 433 (1963).

[9] G.E. Moss, L.R. Miller, R.L. Forward, *Appl. Opt.* **10**, 2495 (1971).

[10] R. Weiss, *Quart. Progr. Rep. Res. Lab. MIT* **105**, 54 (1972).

[11] J. Abadie *et al.*, *Class. Quantum Grav.* **27**, 173001 (2010).

[12] `http://www.virgo.infn.it/`

[13] `http://www.ligo.caltech.edu/`

[14] `http://www.geo600.org/`

[15] `http://tamago.mtk.nao.ac.jp/tama.html`

[16] `http://gw.icrr.u-tokyo.ac.jp/en/`

[17] J. Abadie *et al.*, *Astrophys. J.* **760**, 12 (2012).

[18] J. Abadie *et al.*, *Astro. Astrophys.* **539**, A124 (2012).

[19] B. Abbott *et al.*, *Rep. Prog. Phys.* **72**, 076901 (2009).

[20] T. Accadia *et al.*, *JINST* **7**, P03013 (2012).

[21] L. Blanchet, *Living Rev. Relativity* **9**, 4 (2006).

[22] LIGO Scientific Collaboration, K. Hurley, *Astrophs. J.* **681**, 1419 (2008).

[23] Virgo sensitivity page (accessed 23 November 2013): `https://wwwcascina.virgo.infn.it/DataAnalysis/Calibration/Sensitivity/`

[24] "Advanced Virgo" project home page (accessed 23 November 2013): `http://www.virgo.infn.it/advirgo/`

[25] J. Aasi *et al.*, `arXiv:1304.0670 [gr-qc]`.

[26] K. Somiya, *Class. Quantum Grav.* **29**, 124007 (2012).

[27] P.B. Abbott *et al.* [LIGO Scientific Collaborationand Virgo Collaboration], *Nature* **460**, 990 (2009).

[28] H. Grote *et al.*, *Class. Quantum Grav.* **25**, 114043 (2008).

[29] I. Mandel, R. O'Shaughnessy, *Class. Quantum Grav.* **27**, 114007 (2011).

[30] B. Abbott *et al.*, *Astrophs. J.* **683**, L45 (2008).